Zhang *et al. Biochar* (2025) 7:109
https://doi.org/10.1007/s42773-025-00482-y

Biochar

ORIGINAL RESEARCH

Open Access

Production of carbon dots, biofuels, bio-adsorbents, and biological nutrients via hydrothermal conversion of *Chlorella pyrenoidosa* and oilseed rape straw

Jingmiao Zhang[1,2], Bin Zhang[1,2], Ao Xia[1,2*], Qingming Zhou[1,2], Xianqing Zhu[1,2], Yun Huang[1,2], Xun Zhu[1,2*] and Qiang Liao[1,2]

Abstract

Biomass hydrothermal conversion has received extensive attention due to its advantages of strong adaptability of raw materials, no need to dry feedstock, and relatively mild conditions. *Chlorella pyrenoidosa* (CP) and oilseed rape straw (OS), two kinds of typical biomass, were hydrothermally treated at 230 °C for 6 h to produce carbon dots (CDs), hydrochar (HC), bio-oil (OR), aqueous product (AQ), and volatile product (VO). The CP hydrothermal process generated the highest yield of CDs (16.3%), and the OS hydrothermal process produced the most HC (26.3%). The co-hydrothermal treatment of CP/OS promoted the production of HC and VO via carbonization, decarboxylation, and dehydration reactions between CP and OS degradation products. The CP, OS, and CP/OS based CDs (CD-CP, CD-OS, and CD-CP/OS) in the size of 1.5–26.5 nm emitted blue light and displayed 3.3–11.1% of fluorescence quantum yield. More than 42.3% of methylene blue could be photodegraded by CD-CP, which was 2.1 and 1.4 times higher than that by CD-OS and CD-CP/OS. The higher heating values of HCs and ORs were 23.0–27.8 MJ kg^{-1} and 25.5–38.5 MJ kg^{-1}, showing potential to apply as biofuels. The HCs were confirmed to be outstanding bio-adsorbents that could remove 15.4–68.9% methylene blue with an absorption capacity of up to 275.6 mg g^{-1}. Moreover, the AQs were verified to be potentially used as biological nutrients for microalgae cultivation. This study co-produced CDs, BO, HC, and AQ through the hydrothermal conversion of CP and OS, efficiently utilizing them as photocatalysts, biofuels, bio-adsorbents, and biological nutrients.

Keywords Microalgae, Agricultural straw, Hydrothermal conversion, Carbon dots, Bio-adsorbent, Biological nutrient

*Correspondence:
Ao Xia
aoxia@cqu.edu.cn
Xun Zhu
zhuxun@cqu.edu.cn
Full list of author information is available at the end of the article

Graphical abstract

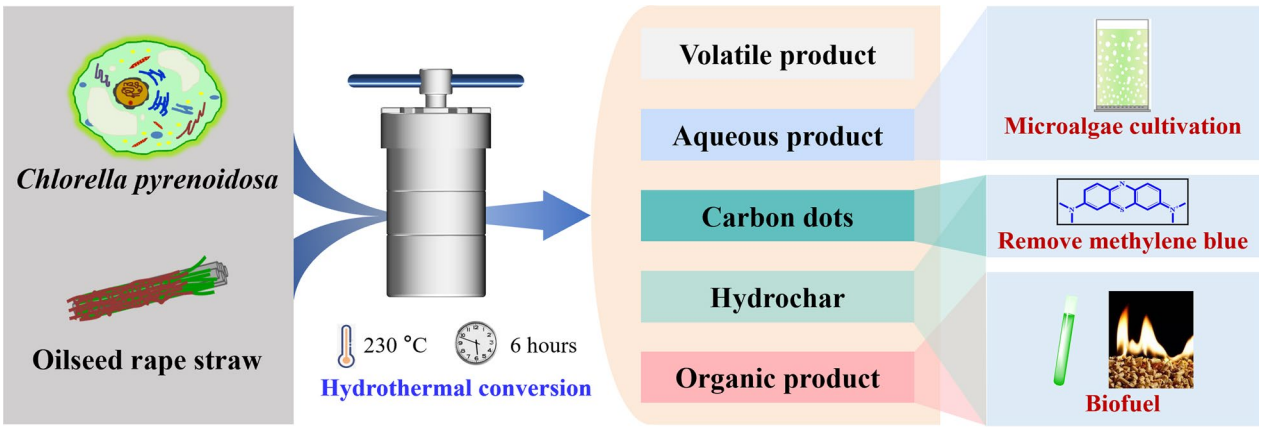

1 Introduction

Biomass is a renewable and abundant resource that can be converted into biofuels, biochar, and other materials for energy production, carbon sequestration, and environmental remediation (Varela et al. 2024). It provides a dual solution to energy scarcity and ecological challenges, supporting sustainable development. Microalgae, which can be sourced from water bloom or large-scale cultivation, are biomass feedstocks with strengths of non-edible crops and non-land requirements. Microalgae have small sizes, fast growth speeds, and high carbon fixation rates (Karimi et al. 2024). Thereby, using microalgae shows tremendous significance in alleviating energy shortages, reducing environmental pollution, and altering resource structure towards the demand for carbon emission reduction. The microalgae, mainly composed of carbohydrates, proteins and lipids, have been used as animal feed and biofertilizer, extracted to obtain high-valued lipids and pigments, and chemically conversed to produce biofuel and biochar (Dahai et al. 2024). Crop straws, the byproduct of the agricultural system with more than one billion tons of annual output in China, play a vital role in the paper-making industry and animal feed traditionally (Sun et al. 2020). In the face of the gain in straw output and decline in their conventional application, open burning has become a common way to dispose of straw, leading to environmental and safety concerns. Governments and researchers have paid much attention to the utilization of straw, including anaerobic digestion, briquet process, thermochemical conversion, and biocomposite preparation (Shi et al. 2022b).

Biomass hydrothermal conversion has attracted extensive attention due to its advantages of strong adaptability of raw materials, no need to dry biomass, and relatively mild conditions (Yu et al. 2024). Solid hydrochar from hydrothermal carbonization has a micron or nanoscale structure, good mechanical properties, and thermal and chemical stability. It could be further applied as biofuels, catalysts, and bio-adsorbents (Chen et al. 2024). The organic bio-oil product has been widely investigated as a substitute for fossil fuels in the petroleum industry. Even though the high N, O, and S heteroatoms in bio-oil have limited its practical application, several works have been conducted to remedy this problem by getting renewable, non-toxic, clean, and alternative fuels (Liu et al. 2022).

In addition to hydrochar and bio-oil, 20–50% of organic components in biomass are transformed into the aqueous phase during hydrothermal carbonization, which is confirmed to contain furan compounds, phenolic derivatives, and organic acids (Usman et al. 2019). The aqueous product with complex composition is challenging to be separated and purified for subsequent use. Meanwhile, it will cause soil/water pollution and organic resource waste problems if discharged directly. Carbon dots (CDs), one kind of zero-dimensional nanomaterials, are generated and exist in the hydrothermal aqueous phase product (Nishshankage et al. 2024; Zhang et al. 2022c). They comprise carbon skeletons with plenty of functional groups, showing unique fluorescence properties, good water solubility, biocompatibility, and electron transfer/storage properties. CDs offer great potential in biosensing, anti-fake, drug delivery, environment monitoring, chemical catalyst, and photoelectric conversion (Zhu et al. 2025).

Recently, the co-hydrothermal conversion of different types of biomass has arisen and been proven to show the merits of reducing residues, improving biofuel properties, and enhancing energy conversion and

carbon retention ratios (daer et al. 2024). Co-hydrothermal carbonization of swine manure and sawdust/corn stalk was found to promote the dehydration of swine manure and enhance the aromatization of hydrochar (Lang et al. 2018). Co-hydrothermal treatment of *Chlorella pyrenoidosa* (CP) and sweet potato residue generated more hydrochar with a higher heating value (HHV). Meanwhile, a positive interaction effect between CP and sweet potato residue was affirmed by verifying a higher energy recovery than the theoretically calculated value (Wang et al. 2019a). However, to our knowledge, the co-hydrothermal process for carbon dots production has not yet been reported. Furthermore, the co-production performance of carbon dots, biofuels, and biomaterials should be compressively investigated to use the multiple hydrothermal products comprehensively.

CP is a protein-rich microalgae species with an ancient history and a short growth cycle (Li et al. 2023). Oilseed rape straw (OS), with more than 4.0 million tons of output in China annually, contains more lignocellulose and low ash than most other agricultural straw (Zhang et al. 2020b). As the carboxyl groups released due to the cleavage of peptide bonds during the reaction process will cause an increase in solution acidity, the introduction of biomass rich in proteins during the hydrothermal process of straw can promote the hydrolysis of cellulose and accelerate the reaction by enhancing the acidic environment (Liu et al. 2022). Moreover, co-hydrothermal carbonization of CP and OS is considered to have the potential to enhance hydrochar yield through aromatization reactions of lignin and cellulose in OS while improving nitrogen retention through the interactions between cellulose, hemicellulose, and proteins in CP (Shen et al. 2024). This study used CP, OS, and CP/OS as substrates for hydrothermal conversion to achieve the clean production of photocatalysts, biofuels, bio-adsorbents, and biological nutrients, thereby improving resource utilization efficiency while broadening the application range of the products. This study aims to:

- Investigate the influence of CP and OS co-hydrothermal conversion on the yields and properties of multiple products.
- Confirm the capacities of CDs, hydrochars, and bio-oils to apply as photocatalysts, biofuels, and bio-adsorbents.
- Identify the potential to reuse the aqueous product as the substrate to cultivate microalgae.

2 Materials and methods

2.1 Materials

The *Chlorella pyrenoidosa* (CP: 32.2%, 48.9%, and 13.4% of carbohydrate, protein, and lipid based on dry weight) powder was purchased from Fuqing King Dnarmsa Co., Ltd. (China). The oilseed rape straw (OS: 51.8%, 26.2%, and 17.5% of cellulose, hemicellulose, and acid-insoluble lignin based on dry weight) powder (40–100 mesh) was obtained from the Tohoku Agricultural Research Center, Japan (Zhang et al. 2020b). CP and OS were dried thoroughly and placed in a dryer for subsequent use. Ethyl acetate and methylene blue (MB), purchased from Shanghai Titan Technology Co., Ltd and Shanghai Macklin Biochemical Co., Ltd, were used for separating hydrothermal products and wastewater treatment experiments.

2.2 Preparation of carbon dots

The CP, OS, or CP/OS (1:1 of mass ratio) powder (w_0: 5 g) was added into a 200 mL hydrothermal autoclave, and 100 mL deionized water was incorporated in the presence of a magnetic stir bar. The autoclave was sealed after replacing the inside air with nitrogen. The mixture was stirred at 250 rpm and heated to 230 °C (5 °C min^{-1}) to run the hydrothermal treatment. The autoclave was cooled sufficiently after the hydrothermal process, which lasted 6 h (Zhang et al. 2022a). The reacted mixture was moved from the opened autoclave and centrifuged at 8000 r min^{-1} for 10 min. The upper solution was collected and ultrafiltrated by a 1000 Da filter membrane to separate the aqueous fraction outside the filter membrane (AQ-p, where p is CP, OS, or CP/OS) and carbon dots fraction inside the filter membrane (CD-p). AQ-p and CD-p were freeze-dried to acquire their dry weights (w_{AQ}, w_{CD}). The bottom sediment was extracted by ethyl acetate, and the residue was referred to as hydrochar fraction (HC-p). HC-p was dried at 60 °C for 24 h and weighed (w_{HC}). The extracted liquid was evaporated to remove ethyl acetate to obtain organic fraction (OR-p) and measured weight (w_{OR}). The volatile fraction (VO-p) weight (w_{VO}) was calculated based on the difference method. The yields of every fraction (Y_{CD}, Y_{HC}, Y_{OR}, Y_{AQ}, and Y_{VO}) were estimated by Eqs. (1) – (5):

$$Y_{CD}(\%) = w_{CD}/w_0 \times 100\% \quad (1)$$

$$Y_{HC}(\%) = w_{HC}/w_0 \times 100\% \quad (2)$$

$$Y_{OR}(\%) = w_{OR}/w_0 \times 100\% \quad (3)$$

$$Y_{AQ}(\%) = w_{AQ}/w_0 \times 100\% \quad (4)$$

$$Y_{VO}(\%) = (w_0 - w_{CD} - w_{HC} - w_{AQ} - w_{OR})/w_0 \times 100\% \quad (5)$$

2.3 Basic analysis of hydrothermal products

The CP, OS, CD-p, OR-p, HC-p, and AQ-p were tested for C, H, N, S, and O elemental contents by a Unicube elementary (Elementar Analysensysteme GmbH, Germany) (Sun et al. 2018). The HHV of CP, OS, OR-p, and HC-p was calculated according to Eq. (6):

$$\mathrm{HHV(MJ\ kg^{-1})} = 0.33858 \times \mathrm{C} + 1.254 \times \mathrm{H} - 0.10868 \times (\mathrm{O} - \mathrm{S}) \quad (6)$$

The CP, OS, CD-p, OR-p, HC-p, and AQ-p were measured for Fourier Transform Infrared Spectrum (FT-IR) using a Nicolet iS50 spectrometer (Thermo Fisher Scientific, USA). The CP, OS, and HC-p powders were coated with gold for 30 s and tested for their microstructures. The scanning electron microscope (SEM) test was conducted on a TESCAN VEGA3 microscope (Tescan Co., Ltd, Czech Republic). CD-p was tested for microstructure by Talos F200S transmission electron microscopy (TEM) (Thermo Fisher Scientific, Netherlands).

CD-p was diluted to get its solution with 0.2 mg L^{-1} of concentration. The solution was tested for UV–visible spectrum using a TU-1950 spectrophotometer (Persee, China). The fluorescence excitation spectrum of CD-p solution was conducted on an FLS1000 stable transient fluorescence spectrometer (Edinburgh Instruments, UK) when excited at 300–500 nm. The fluorescence quantum yield (QY) was also measured when excited at 360 nm.

2.4 Removal of methylene blue by CD-p and HC-p

MB solution was photo-degradingly treated by CD-p under UV light. A 5 mL of deionized water, CD-CP solution, CD-OS solution, or CD-CP/OS solution was added to 95 mL MB solution (10.53 mg L^{-1} of MB) in a 250 mL conical flask. Therefore, the obtained mixtures initially contained 10 mg L^{-1} of MB. The flask was placed in the dark for two hours to reach the adsorption–desorption equilibrium (Rani et al. 2021). Then, the flask was put under UV light to start the photodegradation, and 3.5 mL solutions were taken at the set time to confirm the MB concentration by measuring the absorbance at 665 nm (Liu et al. 2021).

The MB solution was also treated by HC-p, where 25 mg HC-p was added to 100 mL MB solution (10 mg L^{-1} of MB) in a 250 mL conical flask. A blank MB solution without adding hydrochar was also set. The conical flask was placed on the constant temperature magnetic stirrer at 25 °C and 150 rpm to start the absorption experiment (Zhang et al. 2014). Then, 3.5 mL sample suspensions were taken at the required time to measure the MB concentration.

2.5 Cultivation of microalgae by AQ-p

The collected AQ-p was diluted 8 times with deionized water and added in a 500 mL serum bottle to culture microalgae *Chlorella vulgaris* FACHB-31. The quantified pre-cultured *C. vulgaris* was added to the bottle, and its inoculation concentration was around 0.1 g L^{-1}. The microalgae were cultured for 8 days at 25 ± 1 °C. The light intensity was 97 ± 3 μmol m^{-2} s^{-1} for 24 h, and the aeration rate was 0.1 vvm of 10% CO_2 (Zhang et al. 2022b). The microalgae concentration and solution pH were detected daily by dry weight method and FG2 portable pH meter (Mettler-Toledo, Switzerland).

3 Results and discussion

3.1 Hydrothermal products distribution

The yields of hydrothermal products from CP, OS, and CP/OS hydrothermal systems are shown in Fig. 1. CP as feedstock produced the most CDs, up to 16.3%, indicating microalgae had unique advantages as raw materials to prepare CDs. The Maillard reaction among carbohydrates and proteins hydrolysis products was proven to significantly influence the generation of CDs (Zhang et al. 2022a). The yield of CD-OS was only 6.3%, while the yield of CD-CP/OS was 10.8%, showing the feasibility of CDs production via the hydrothermal treatment of CP/OS. The CP contains 32.2% and 48.9% carbohydrate and protein, where their hydrolysis products will undergo Maillard reaction during the hydrothermal process. The 51.8% cellulose and 26.2% hemicellulose in OS could also generate sugars to participate in the Maillard reaction. However, during CP/OS co-hydrothermal treatment, the components required to produce amino acids for the Maillard reaction might be inadequate, as another kind of

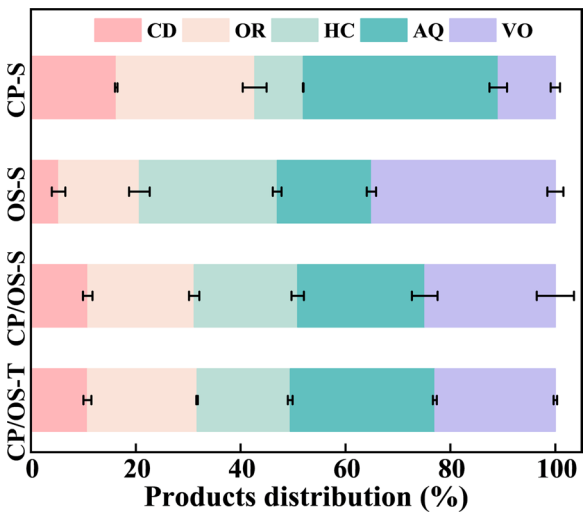

Fig. 1 Hydrothermal products distribution

reactant, sugars, could be generated from carbohydrates in CP, cellulose and hemicellulose in OS. Therefore, the co-hydrothermal treatment of CP/OS produced fewer CDs than CP hydrothermal process. The yield of CD-p was higher than 0.75% of CDs prepared from *Enteromorpha prolifera* with microwave-assisted hydrothermal treatment for 30 min at 200 °C (Wang et al. 2019b), but lower than 20% of wheat straw-based CDs when hydrothermally heated at 250 °C for 10 h (Yuan et al. 2015). It implied that the difference in CD yields was caused by different feedstocks and simultaneously related to the hydrothermal conditions.

The CP hydrothermal system produced higher yields of OR and AQ, but less HC and VO than OS system (Fig. 1). The lignocellulosic straw was more challenging to decompose than microalgae because the hydrophobicity and cross-linked aromatic lignin would interfere with hydrolysis (Sankaran et al. 2020). It leads to more dissolved components and less residue after CP hydrothermal treatment than OS hydrothermal treatment, resulting in more OR and AQ, but less HC in CP system than OS system. Moreover, microalgae lipids contributed to producing more OR-CP during hydrothermal conversion (Tsarpali et al. 2021). The high yield of VO-OS (35.1%) was mainly in connection with the decomposition of a portion of hemicellulose and small molecules to release volatile content (Yu et al. 2021).

Figure 1 shows that the yields of all fractions from the CP/OS system were in the middle when compared with CP and OS systems, respectively. A similar finding was also observed when rice straw and sewage sludge were co-hydrothermally treated at 200 °C for 2 h (Zhang et al. 2020c). The product distribution in CP/OS theoretical system (CP/OS-T) was estimated by the average product distribution in CP system and OS system (Fig. 1). The experimental yields of CD and OR in CP/OS system were consistent with those in CP/OS-T. However, the experimental HC and VO yields were higher than their theoretical yields, while the practical AQ yield was lower than its theoretical yield. It is assumed that a mix of CP and OS could promote the production of solid and volatile fractions via carbonization, decarboxylation, and dehydration reactions between CP and OS during hydrothermal treatment, which was the same as in woody sawdust and food waste co-hydrothermal carbonization (Wang et al. 2020). The synergistic effect of CP and OS promotes the generation of numerous small molecules during the co-HTC process, which are present in AQ. Some of these compounds, such as N-containing organic compounds and ammonium salts, are captured and polymerized at the solid–liquid interface by carbohydrates and their derivatives, forming additional secondary char (Shen et al. 2024). Meanwhile, other substances with lower boiling points are converted into volatile compounds, contributing to an increased yield of volatile products.

3.2 Elemental composition

The CP contained a higher C content and lower O content than OS, leading to a higher HHV of CP (19.5 MJ kg^{-1}) than OS (17.9 MJ kg^{-1}) (Fig. 2a, f). However, natural microalgae always contain high moisture, which impedes their direct use as suitable biofuel. The CP included 6.9% of N as its protein components, higher than 0.6% of OS, which could contribute to the production of N-doped carbon materials for application. As shown in Fig. 2b, the CD-CP included 8.5% of N, higher than 1.6% of CD-OS, which might enhance the luminescence property of CDs (Liao et al. 2024). Furthermore, the high N content led to a lower O content in CD-CP than in CD-OS, owing to water loss via carboxylic acid and amino group condensation (Liang et al. 2021). The CD-CP/OS contained 7.0% of N, higher than the average N content of CD-CP and CD-OS, indicating that the co-hydrothermal process promoted N doping onto CDs. Furthermore, the CD-CP/OS contained a super high H content and a unique low O content compared to other CDs, implying the lower aromaticity and fewer O-containing groups in CD-CP/OS caused by the interactions between CP and OS. The high doping N content in CD-CP/OS could make CDs have better photoluminescence property, while the low O content might reduce the water solubility of CD-CP/OS and make the modification of CD-CP/OS difficult (Zhang et al. 2022c).

Compared with raw materials (Fig. 2a, c), the C content increased while N and O contents decreased in OR-p after the hydrothermal treatment via denitrification and deoxygenation reactions (Huang et al. 2016). In Fig. 2c, f, OR-CP shows 38.5 MJ kg^{-1} of HHV and contains higher C, H, and S contents but a lower O content than OR-OS. It indicated that microalgae-based bio-oil was more outstanding for application as bio-fuel than lignocellulosic straw-based bio-oil (Lu et al. 2022). The HHV of OR-CP was somewhat lower than 42 MJ kg^{-1} of petroleum crude oil and slightly higher than 33.9–36.5 MJ kg^{-1} of *Bacillariophyta* sp. and *Cyanobacteri*a sp. hydrothermal bio-oil (Huang et al. 2016), showing a potential to be used as biofuels. The HHV of OR-CP/OS was lower than the average of OR-CP and OR-OS, suggesting no synergistic effect on bio-oil HHV between CP and OS at a hydrothermal temperature of 230 °C, likely due to insufficient temperature to enhance bio-oil yield or quality.

In terms of HC-p, they contained 53.5–64.7% C, 1.7–4.0% N, 5.9–7.2% H, 0.4–1.3% S, and 24.8–35.2% O (Fig. 2d). The C content in HC-p increased, and the O content decreased after the hydrothermal process due to the occurrence of deoxygenation reactions (Xu et al.

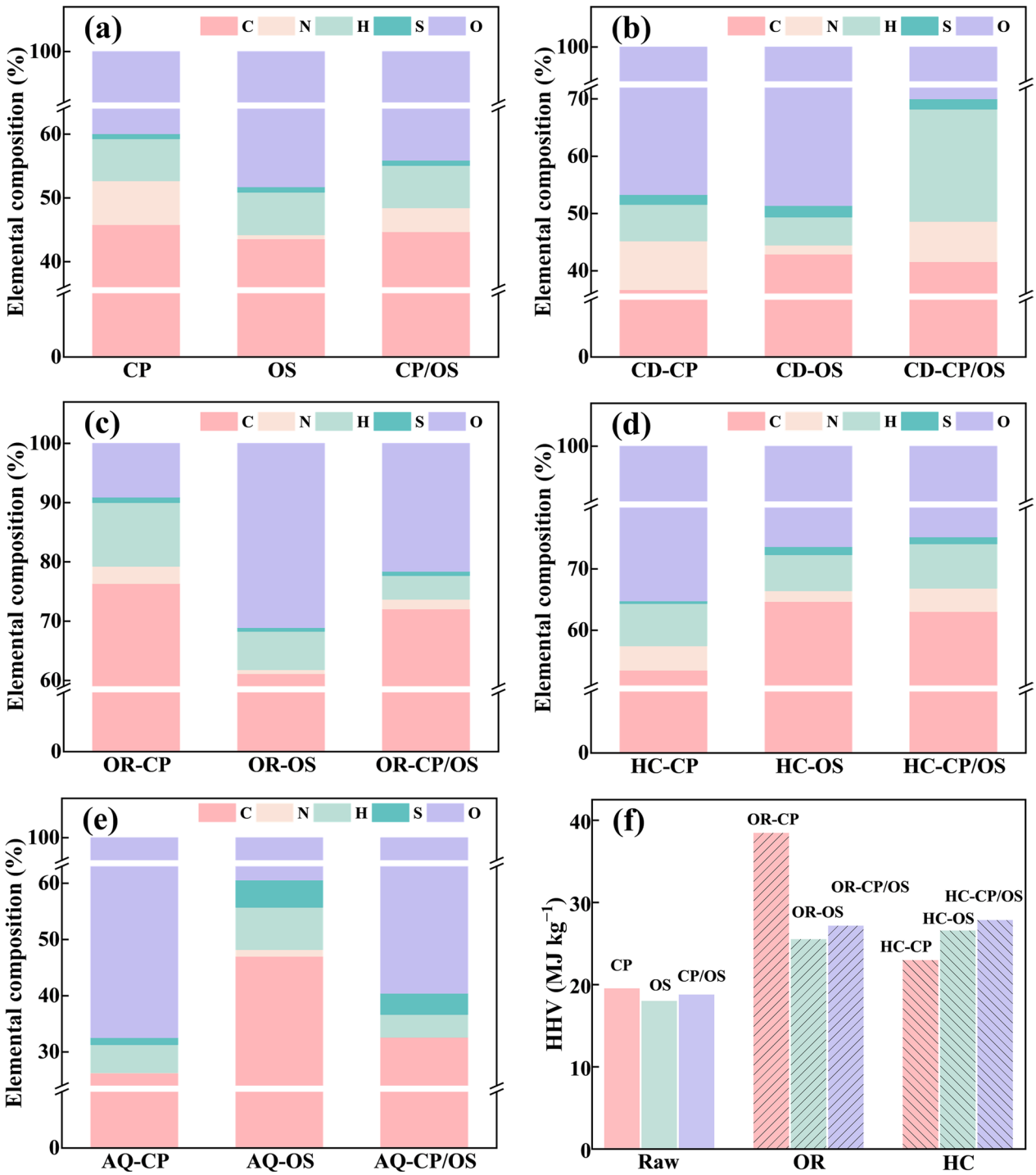

Fig. 2 Elemental composition and higher heating value of feedstocks and hydrothermal products. **a** Elemental composition of feedstocks, **b** carbon dots, **c** bio-oil, **d** hydrochar and **e** aqueous product; **f** Higher heating value of feedstocks and hydrothermal products

2019). A similar trend was also observed in the hydrothermal carbonization of corn cob, rice husk, and tobacco stalk (Li and Cai 2022; Xu et al. 2019). As to N content, HC-CP showed a lower N content than CP, while the N content in HC-OS increased by approximately 1.8 times after the hydrothermal process. The decreased N content in HC-CP was due to the dissolution of the microalgal protein components (Miyata et al. 2022), and the

dissolved N was confirmed to tend to dope onto CD-CP. The HHV of HC-p ranged from 23.0 to 27.8 MJ kg^{-1}, with HC-CP/OS exhibiting a higher HHV than both HC-CP and HC-OS (Fig. 2f), surpassing not only the sludge/saw dust hydrochar (14.0 MJ kg^{-1}) (Zhang et al. 2023b), but also water hyacinth/sewage sludge hydrochar (19.6 MJ kg^{-1}) (Zhang et al. 2020a). The obtained HC-p contained 0.4–1.3% S, lower than 0.6–1.4% of lignite, showing that HC-CP as an alternative solid fuel helps reduce SO_x emission to the atmosphere (Lee et al. 2018).

The AQ-p contained 26.3–47.0%, 0–1.2%, 4.0–7.5%, 1.3–4.8%, and 39.4–67.4% of C, N, H, S, and O, respectively (Fig. 2e). The AQ-OS included higher C, N, H, and S contents but a lower O content than AQ-CP and AQ-CP/OS, which might relate to the generation of vast oxygen-containing volatiles during the OS hydrothermal process.

3.3 FTIR

As shown in Fig. 3a, CP and OS contained large amounts of O–H and N–H (3720–3000 cm^{-1}), C–H (3000–2810 cm^{-1} and 1500–1325 cm^{-1}), C=O and C=C (1800–1500 cm^{-1}), C–O and C–C (1200–960 cm^{-1}) bonds (Zhang et al. 2020b). Because of the lignin components, OS contained aromatic structures and displayed more substantial peaks in 1700–1500 cm^{-1}. The C=O (1800–1700 cm^{-1}) and C–O (1200–960 cm^{-1}) peaks in OS were more noticeable due to the higher O content in OS than that in CP (Fig. 2a).

The FTIR of CD-p showed peaks of O–H, N–H, C–H, C=O, C=C, C–O, and C–C as well, verifying the abundant functional groups contained in CD-p (Fig. 3a). The N–H (3300–3000 cm^{-1}) peak in CD-CP was higher than that in CD-OS and CD-CP/OS, which was consistent with their N contents (Fig. 2b) (Sui et al. 2014). The C=O (1800–1700 cm^{-1}) peak in CD-OS was observed, while it had not been identified in CD-CP and CD-CP/OS, indicating the presence of carbonyl groups in CD-OS (Wang et al. 2015). In terms of C=C, the CD-CP showed hugely high C=C peaks, while C=C peaks in CD-OS were the lowest, which might relate to the highest aromaticity of CD-CP structure and the lowest aromaticity of CD-OS structure.

As to OR-p, OR-OS and OR-CP/OS showed an O–H peak at 3670–3020 cm^{-1}, while the OR-CP displayed an N–H peak at 3470–3130 cm^{-1} (Fig. 3b). The absence of O–H peak in OR-CP might be caused by the fact that the major components of microalgae-based bio-oil were N-containing heterocyclic compounds (Zhang et al. 2023a). The O–H peak that appeared in OR-OS and OR-CP/OS was attributed to their phenolic compounds (García et al. 2017). The peaks around 3000–2810 cm^{-1} and 1500–1325 cm^{-1} belonging to C–H bonds demonstrated the existence of alkane groups in these bio-oils (Ji et al. 2017; Singh et al. 2014). In terms of C=O and C=C bonds (1800–1500 cm^{-1}), the OR-p showed prominent peaks belonging to ketones, aldehydes, and esters in these bio-oils (Ji et al. 2017; Singh et al. 2014).

The weak O–H, C=O, and C=C peaks in HC-CP derivate from CP implied that microalgae CP had adequately decomposed during hydrothermal processes (Fig. 3b) (Huang et al. 2016). However, these peaks in HC-OS were still kept as the hydrothermal temperature at 230 °C was not enough to fully degrade the macromolecules in OS

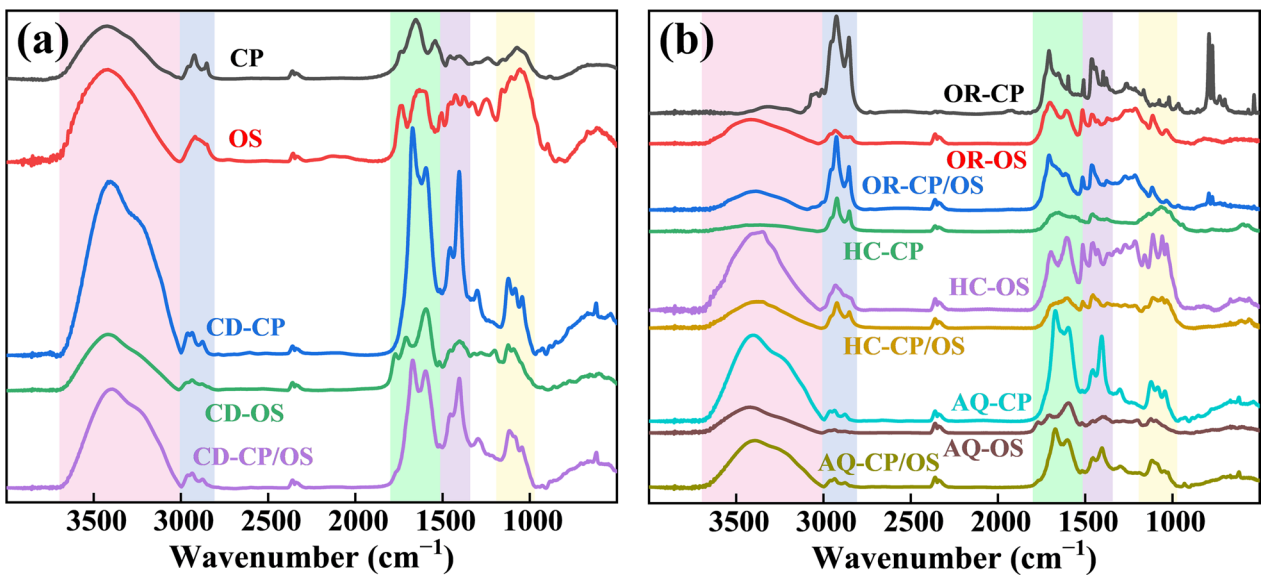

Fig. 3 FTIR of feedstocks and hydrothermal products. **a** Feedstocks and carbon dots; **b** bio-oil, hydrochar, and aqueous product

(Dutta et al. 2022). These absorption peaks in HC-CP/OS were moderate when compared with HC-CP and HC-OS, indicating that the co-hydrothermal treatment of CP/OS could result in HC with fewer functional groups or less degradable structures than the hydrothermal treatment of OS.

Regarding AQ-p, the O–H, N–H, C–H, C=O, C=C, C–O, and C–C peaks also appeared (Fig. 3 a, b), which were assigned to amines, N-heterocycles, short-chain acids, alcohols, and volatile fatty acid contained in AQ-p (Zhu et al. 2017). The C=O (1800–1740 cm^{-1}) peak in AQ-OS was more evident than in AQ-CP or AQ-CP/OS, indicating the presence of more carboxyl-containing compounds, such as carboxylic acids, ketones, and aldehydes. These carboxyl-containing compounds were produced by serial reactions such as cellulose hydrolysis, glucose dehydration, and intermediates hydrolysis (Gao et al. 2012).

3.4 SEM

The CP is composed of 4–30 μm spheres with many wrinkled structures on their surfaces (Zhang et al. 2022a), while 40–100 mesh OS consists of strips with fold structures and small holes in the interior (Cui et al. 2017) (Fig. 4a, b). These wrinkled, fold and multi-hole structures of CP and OS could give them large specific surface areas, which would be conducive to transfer and contact between substances during hydrothermal processes.

The CD-CP and CD-OS were 13.5–26.5 nm and 1.5–3.7 nm, respectively, while the size of CD-CP/OS was 1.6–5.5 nm (Fig. 4c–e). The bigger CD-CP might be on account of the proteins in microalgae (Zhang et al. 2022c). The size of CD-CP was smaller than the average size of *Pectinodesmus* sp. hydrothermal CDs (Amjad et al. 2019) and 20.0–50.0 nm of *Spirulina* hydrothermal CDs of 67.0 nm (Zhang et al. 2019), but bigger than the 3.2 nm of *Dunaliella salina* hydrothermal CDs (Amjad et al. 2019). On the other hand, the size of CD-OS was similar to the average size of wheat straw hydrothermal CDs (Shi et al. 2022a) and 1.1–4.0 nm of flax straw hydrothermal CDs of 1.7 nm (Hu et al. 2020). Regarding CD-CP/OS, it was confirmed that the co-hydrothermal treatment conduced to the production of CDs in smaller sizes than CD-CP, which might contribute to their subsequent applications.

Regarding HC-p, they exhibited irregular shape and size, and raw materials morphology had disappeared because their structures were destroyed by hydrothermal treatment (Fig. 4f–h). The HC-CP exhibited more hollow structures than HC-OS, which might arise from the more complete decomposition of CP relative to OS. The HC-CP/OS microstructure was more like HC-OS because microalgae were easier to decompose, and fewer microalgae-derived residues remained during the co-hydrothermal process.

3.5 Optical properties

These CD-p solutions exhibited strong absorption in the UV range between 200 and 400 nm, emitting blue light under UV illumination (Fig. 5a). Like many CDs (Zulfajri et al. 2021), the CD-CP solution showed two absorption peaks at 270 nm and 325 nm. The former was due to the $\pi-\pi^*$ transition of C=C bonds from aromatic constituents, and the latter is related to the $n-\pi^*$ transition of N- or O-containing groups (Shi et al. 2022a; Zhang et al. 2022a). The CD-OS solution displayed an absorption peak at 270 nm while the peak at 325 nm was not prominent, which might be a result of the small amount of N-containing groups contained in CD-OS (Fig. 2b). The CD-CP/OS solution also had the above two peaks, indicating the co-hydrothermal process could contribute to generating N-doped CDs (Ruan et al. 2016).

As to the fluorescence emission spectrum, CD-p solutions displayed excitation wavelength-dependent and bathochromic-shifted fluorescence behavior (Fig. 5b-d). It was considered related to the particle size and surface states (such as the N-states and O-states) of CDs near the Fermi level (Zhang et al. 2022c). The CD-CP and CD-CP/OS showed maximum fluorescence intensity at 430 nm with excitation at 340 nm. The CD-OS showed the lowest fluorescence intensity at 440 nm with excitation at 360 nm. It was consistent with the stronger emitted blue light of CD-CP and CD-CP/OS than CD-OS under UV illumination (Fig. 5a).

The QY of CD-CP, CD-OS, and CD-CP/OS was 11.1%, 3.3%, and 9.4%, respectively. It was conjectured that microalgae were more applicable than lignocellulose to prepare CDs with higher QY when hydrothermally treated at 230 °C. Because the microalgae components were easier to dissolve and degrade than lignocellulose under the hydrothermal temperature of 230 °C (Lu et al. 2022). Furthermore, the abundant nitrogen in microalgae could promote the production of CDs doping with N. The higher nitrogen content doped onto CDs has been proven to make the CDs display better fluorescent properties (Zhang et al. 2022a). Compared with other works, the QY of these CDs is higher than 4.8% of corn stover-based CDs and 8.0% of *Dunaliella salina*-based CDs (Singh et al. 2019; Yang et al. 2021).

3.6 Degradation and adsorption of methylene blue by CD-p and HC-p

After 450 min of UV irradiation in MB aqueous solution, CD-CP, CD-OS, and CD-CP/OS achieved MB

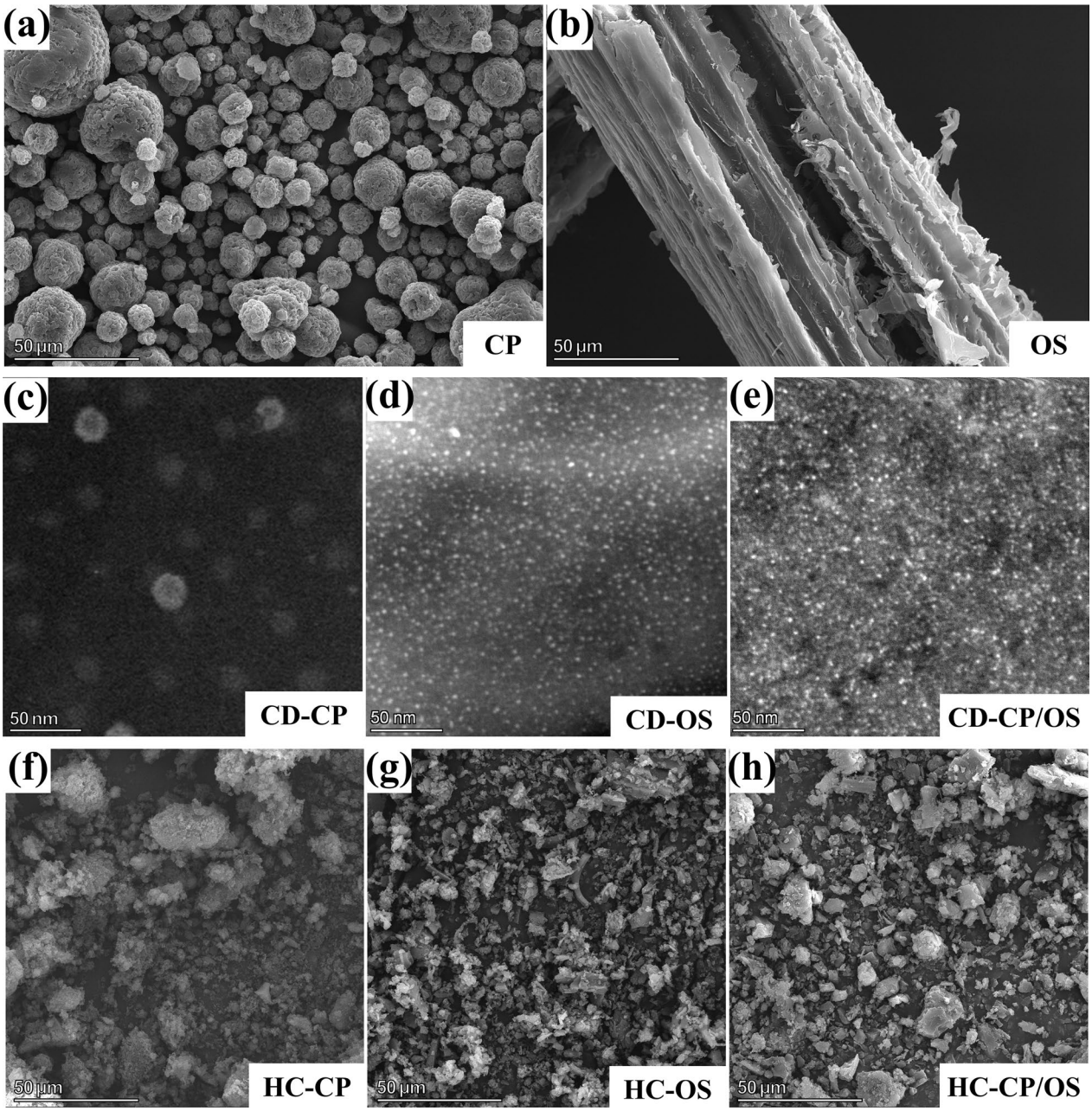

Fig. 4 Microstructure of feedstocks and products. **a**, **b** SEM of feedstocks; **c**–**e** TEM of carbon dots; **f**–**h** SEM of hydrochar

degradation efficiencies of 42.3%, 19.7%, and 29.5% respectively, significantly exceeding the12.4% of blank sample (Fig. 6a). CD-CP exhibited the highest performance in photodegrading MB due to its strongest fluorescence resulting from the highest QY, whereas CD-OS showed the weakest photodegradation ability, corresponding to its lowest QY and weakest fluorescence. Compared with some other biomass-derived carbon dots, such as those from birch residue (with a degradation rate of 37.0%) (Jia et al. 2024), CD-p exhibits higher photocatalytic degradation ability, yet it is still lower than that of CD composites. For example, the removal rate of methylene blue (MB) by the CD/g-C_3N_4 heterojunction can reach 94.6% (Liu et al. 2021). Generally, it is assumed that the prepared CD-p exhibits the ability to photodegrade MB, and that the degradation ability is positively correlated with its fluorescence properties. CDs could contribute to forming additional electron–hole pairs to absorb

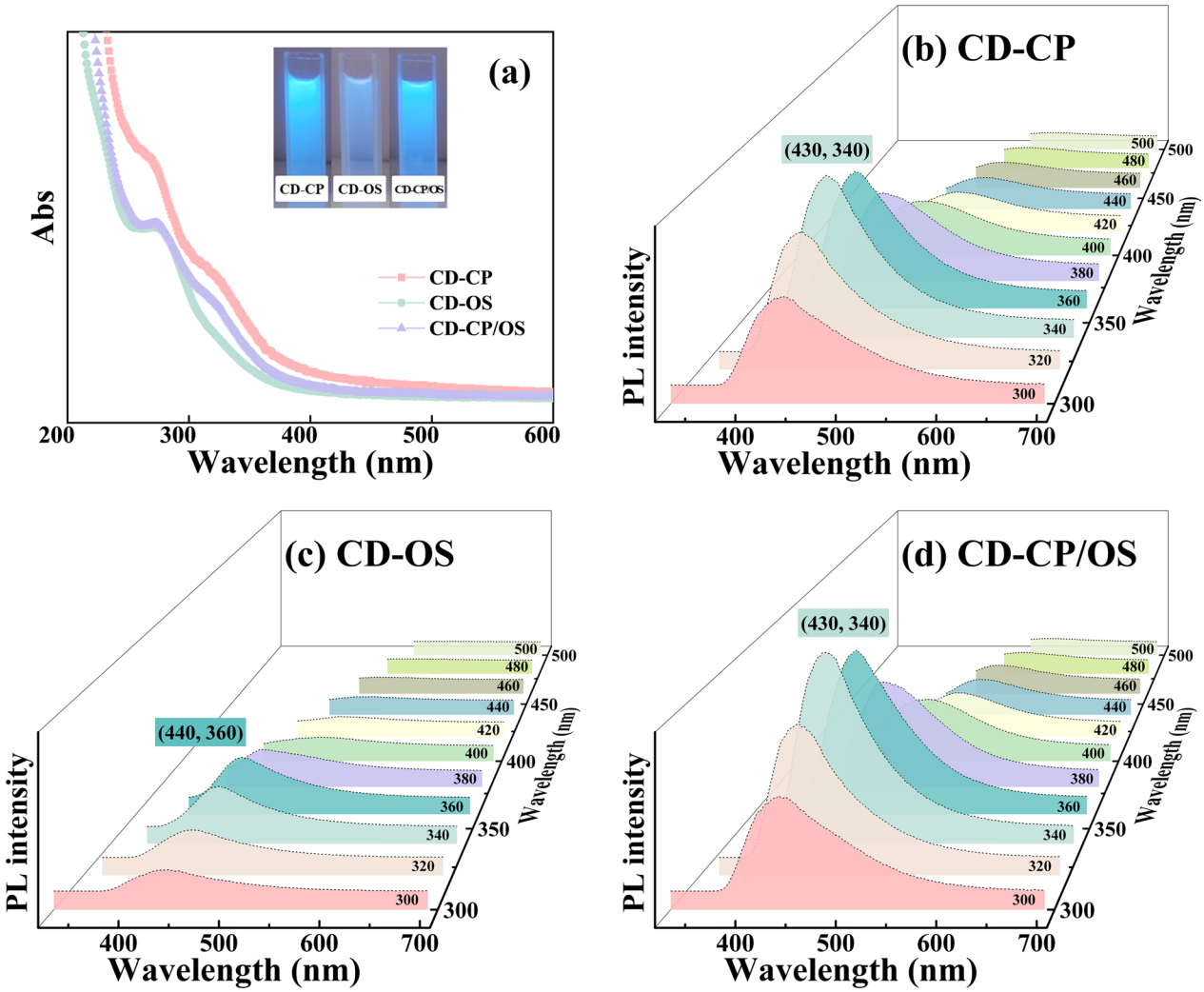

Fig. 5 UV–Vis absorption and fluorescence emission spectra of carbon dots. **a** UV–vis absorption spectra of carbon dots; **b**–**d** Fluorescence emission spectra of carbon dots

more entire spectra. Meanwhile, CDs as electronic acceptors could enrich electron transfer and reduce the recombination of photo-generated charge carriers for generating more heterojunctions to degrade MB (Zhang et al. 2022c).

In terms of HC-p, HC-CP, HC-OS and HC-CP/OS removed more than 15.4%, 68.9% and 27.1% of MB, respectively, while the blank sample removed 6.2% after 450 min of treatment (Fig. 6b). The HC-OS displayed the highest MB removal efficiency, demonstrating remarkable adsorption capacity for potential use as an adsorbent. The hemicellulose, amorphous cellulose, and amorphous cellulose are partially hydrolyzed at 230 °C, thus forming a rough and porous network structure of the obtained HC-OS (Li et al. 2021a). The absorption capacity of HC-OS reached 275.6 mg g^{-1}, which was higher than 155.1 mg g^{-1} of mason pine-derived hydrochar (Zhang et al. 2024), comparable with 259.0 mg g^{-1} of bamboo/polyvinyl chloride hydrochar (Li et al. 2021b), but lower than 340.3 mg g^{-1} of distiller grains/clay minerals hydrochar (Xu et al. 2021). The co-hydrothermal treatment of CP and OS did not improve the MB absorption capacity of hydrochar in this study. Still, it increased the HHV of HC-CP/OS, indicating the hydrothermal conversion of OS was more suitable for preparing hydrochar for absorbent application. In contrast, co-hydrothermal treatment of CP and OS was beneficial in producing hydrochar for biofuel applications (Table 1).

3.7 Microalgae cultivation by AQ-p

As shown in Fig. 7a, the AQ-CP showed the best ability to cultivate microalgae *Chlorella vulgaris*, and the microalgae productivity could reach 1.1 g L^{-1} after culturing

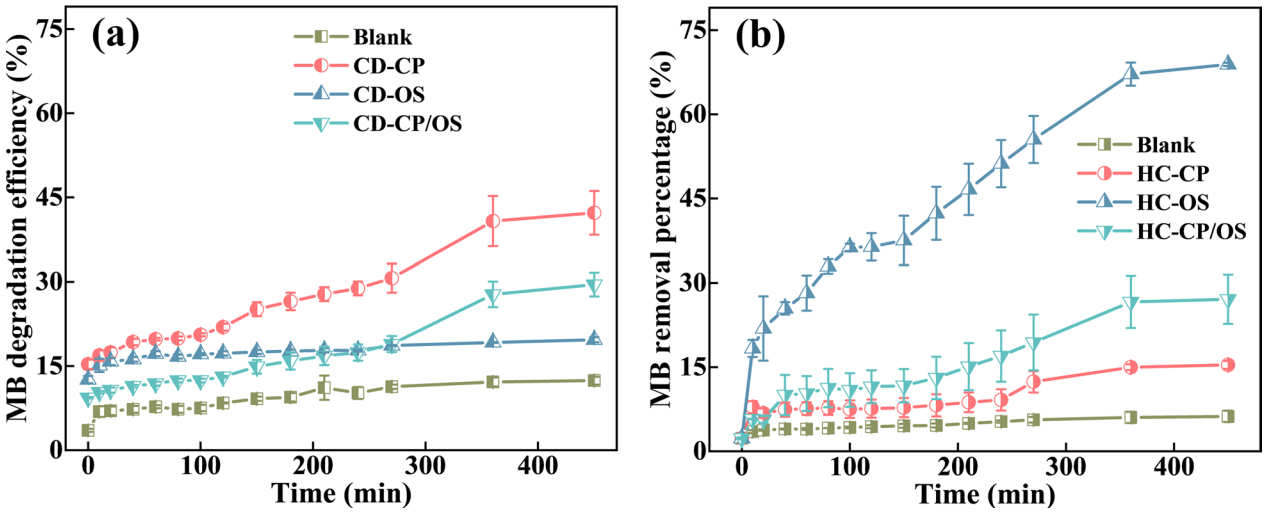

Fig. 6 Degradation and adsorption of methylene blue via carbon dots (**a**) and hydrochars (**b**)

in AQ-CP medium for 8 days, higher than 0.4 g L^{-1} of AQ-CP/OS. The co-hydrothermal treatment of CP and OS could make the AQ more usable for biomass cultivation than OS hydrothermal treatment. The growth rate of *C. vulgaris* in AQ-CP was up to 0.2–0.3 g L^{-1} d^{-1} at the beginning two days, and the growth speed slowed down with prolonged cultivation time. It demonstrated that the compounds in AQ-CP could initially be used as nutrients for growth, and then the decrease in available nutrients would slow down the growth of microalgae. When compared with other studies, the microalgae productivity in this study was higher than 0.7 g L^{-1} of *Chlorella minutissima* cultured in municipal sludge hydrothermal aqueous phase (Kumar et al. 2021), and 0.6 g L^{-1} of microalgae (*Chlorella* sp.)-fungi (*Penicillium* sp.) cultured in microalgae-fungal hydrothermal aqueous phase (Chen et al. 2020). Generally, the AQ-CP was the most suitable medium to culture *C. vulgaris* among these three produced aqueous products, which could help solve the hydrothermal wastewater problem and recycle the nutrients in the aqueous phase.

However, *C. vulgaris* almost could not grow in AQ-OS, which might be due to the low pH of AQ-OS throughout the cultivation. The diluted AQ-OS medium showed a pH of approximately 4.4 because of the presence of vast volatile fatty acids (Fig. 7b), which were produced from the hydrolysis of hemicellulose and cellulose (Zhu et al. 2017). The pH of AQ-CP and AQ-CP/OS mediums first increased and then stabilized during the *C. vulgaris* cultivation process (Fig. 7b). The increased trend of pH was the accumulation of hydroxyl ions generated from microalgae photosynthesis (Tsarpali et al. 2021).

Table 1 The degradation or adsorption capacity of materials derived from other biomass sources

Precursor of carbon dots	Material type	Degradation ability (%)	References
Degradation			
Corncob lignin	CD composites	94.6	Liu et al. (2021)
Glucose	CD composites	90.1	Yao et al. (2018)
Residue of birch	CDs	37.0	Jia et al. (2024)
CP	CDs	42.3	This study
Precursor of biochar	**Fabrication process**	**Adsorption ability (mg g^{-1})**	**References**
Adsorption			
Eucheuma cottonii Seaweed	Pyrolysis	133.3	Saeed et al. (2020)
Mason pine	Hydrothermal carbonization	155.1	Zhang et al. (2024)
Polyvinyl chloride/bamboo	Co-hydrothermal carbonization	259.0	Li et al. (2021b)
Distiller grains/clay minerals	Co-hydrothermal carbonization	340.3	Xu et al. (2021)
OS	Hydrothermal carbonization	275.6	This study

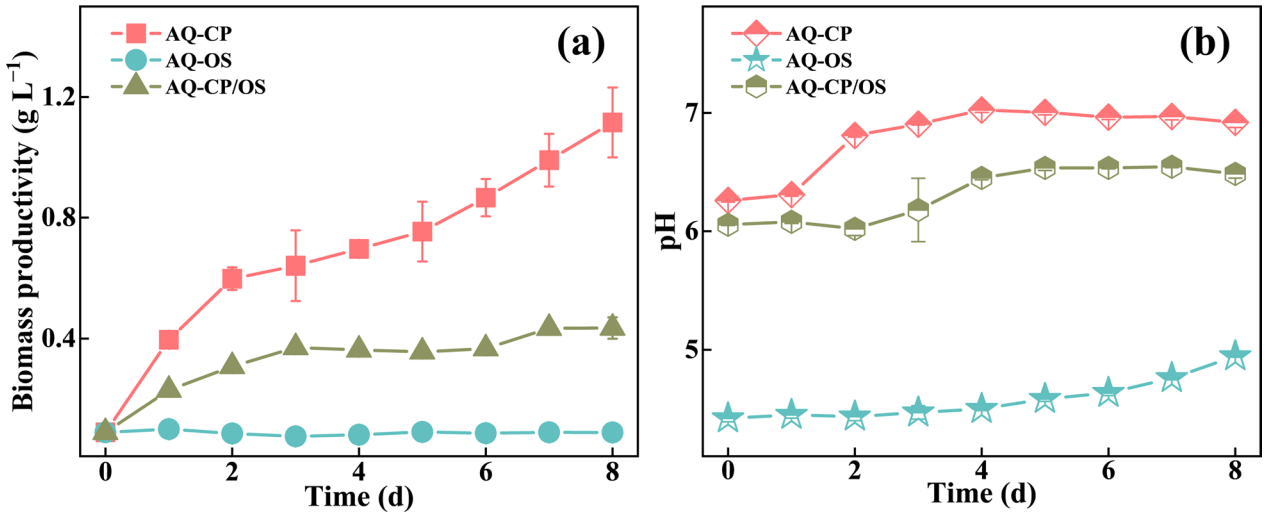

Fig. 7 Biomass productivity (**a**) and pH (**b**) during microalgae cultivation in aqueous product

4 Conclusion

The hydrothermal conversions of CP, OS, and CP/OS were investigated for the clean production of CDs, biofuels, bio-adsorbents, and biological nutrients, which could enhance resource utilization efficiency. The CP hydrothermal process had more CD, OR, and AQ, but less HC and VO than the OS hydrothermal process. The CP/OS co-hydrothermal treatment generated more HC and VO but less AQ via carbonization, decarboxylation, and dehydration reactions between CP and OS degradation products. CD-CP, CD-OS, and CD-CP/OS sizes were 13.5–26.5 nm, 1.5–3.7 nm, and 1.6–5.5 nm, emitting blue light under UV illumination and showing 3.3–11.1% of QY. The highest HHVs of bio-oil and hydrochar were 38.5 MJ kg^{-1} of OR-CP and 27.8 MJ kg^{-1} of HC-CP/OS, indicating their potential for biofuel use. The CD-CP could photodegrade 42.3% MB, higher than CD-OS and CD-CP/OS, due to its more potent fluorescence property. The HC-OS could remove 68.9% of MB and displayed an MB absorption capacity of up to 275.6 mg g^{-1}. The AQ-CP showed the best ability to cultivate *C. vulgaris* with 1.1 g L^{-1} of microalgae productivity, higher than 0.4 g L^{-1} of AQ-CP/OS, while the *C. vulgaris* almost could not grow in AQ-OS. The CP hydrothermal conversion was more suitable for producing CDs, liquid biofuel, and reusable aqueous products. The OS hydrothermal conversion was preferable for preparing bio-adsorbents, while the CP/OS co-hydrothermal conversion demonstrated superior performance for preparing solid biofuels. However, the interactions between CP and OS during the hydrothermal process require further analysis, and the performance of the individual products needs to be enhanced.

Abbreviations

AQ	Aqueous product
CDs	Carbon dots
CP	*Chlorella pyrenoidosa*
CP/OS-T	CP/OS theoretical hydrothermal system
FT-IR	Fourier transform infrared spectrum
HC	Hydrochar
HHV	Higher heating value
MB	Methylene blue
OR	Bio-oil
OS	Oilseed rape straw
QY	Quantum yield
SEM	Scanning electron microscope
TEM	Transmission electron microscopy
VO	Volatile product

Author contributions

Jingmiao Zhang: Investigation, Data curation, Writing – original draft. Bin Zhang: Investigation, Writing – original draft. Ao Xia: Conceptualization, Supervision, Writing – review & editing. Qingming Zhou: Investigation. Yun Huang: Investigation. Xianqing Zhu: Investigation. Xun Zhu: Supervision, Writing – review & editing. Qiang Liao: Writing – review & editing. The author(s) read and approved the final manuscript.

Funding

This work was supported by the National Natural Science Foundation of China (Nos. 52236009, 52106224), the Innovative Research Group Project of the National Natural Science Foundation of China (No. 52021004), the Natural Science Foundation of Chongqing (Nos. CSTB2023NSCQ-JQX0005), the Venture & Innovation Support Program for Chongqing Overseas Returnees (No. cx2022027), and Key Laboratory of Low-grade Energy Utilization Technologies and Systems permanent staff research fund (LLEUTS 2024001).

Data availability

The datasets used or analyzed during the current study are available from the corresponding author upon reasonable request.

Declarations

Competing interests
The authors declare that they have no known competing financial interests or personal relationships that could have appeared to influence the work reported in this paper.

Author details
[1]Key Laboratory of Low-Grade Energy Utilization Technologies and Systems, Ministry of Education, Chongqing University, Chongqing 400044, China. [2]Institute of Engineering Thermophysics, School of Energy and Power Engineering, Chongqing University, Chongqing 400044, China.

Received: 29 November 2024 Revised: 27 April 2025 Accepted: 11 June 2025
Published online: 11 September 2025

References

Amjad M, Iqbal M, Faisal A, Junjua AM, Hussain I, Hussain SZ, Ghramh HA, Khan KA, Janjua HA (2019) Hydrothermal synthesis of carbon nanodots from bovine gelatin and PHM3 microalgae strain for anticancer and bioimaging applications. Nanoscale Adv 1(8):2924–2936

Chen J, Ding L, Liu R, Xu S, Li L, Gao L, Wei L, Leng S, Li J, Li J, Leng L, Zhou W (2020) Hydrothermal carbonization of microalgae-fungal pellets: removal of nutrients from the aqueous phase fungi and microalgae cultivation. ACS Sustain Chem Eng 8(45):16823–16832

Chen Z, Guo Y, Luo L, Liu Z, Miao W, Xia Y (2024) A critical review of hydrochar based photocatalysts by hydrothermal carbonization: synthesis, mechanisms, and applications. Biochar 6(1):74

Cui LQ, Chen TM, Quan GX, Xiao B, Ma YR, Pan M, Liu Y, Liu BZ, Yin CT, Yan JL, Han XY, Ding C, Cui J, Bian MJ, Hussain Q (2017) Renewable material-derived biochars for the efficient removal of 2,4-dichlorophen from aqueous solution: adsorption/desorption mechanisms. BioResources 12(3):4912–4925

Daer D, Luo L, Shang Y, Wang J, Wu C, Liu Z (2024) Co-hydrothermal carbonization of waste biomass and phosphate rock: promoted carbon sequestration and enhanced phosphorus bioavailability. Biochar 6(1):70

Dahai H, Zhihong Y, Lin Q, Yuhong L, Lei T, Jiang L, Liandong Z (2024) The application of magical microalgae in carbon sequestration and emission reduction: removal mechanisms and potential analysis. Renew Sustain Energy Rev 197:114417

Dutta S, Yu IKM, Fan J, Clark JH, Tsang DCW (2022) Critical factors for levulinic acid production from starch-rich food waste: solvent effects, reaction pressure, and phase separation. Green Chem 24(1):163–175

Gao Y, Wang X-H, Yang H-P, Chen H-P (2012) Characterization of products from hydrothermal treatments of cellulose. Energy 42(1):457–465

García T, Veses A, López JM, Puértolas B, Pérez-Ramírez J, Callén MS (2017) Determining bio-oil composition via chemometric tools based on Infrared spectroscopy. ACS Sustain Chem Eng 5(10):8710–8719

Hu G, Ge L, Li Y, Mukhtar M, Shen B, Yang D, Li J (2020) Carbon dots derived from flax straw for highly sensitive and selective detections of cobalt, chromium, and ascorbic acid. J Colloid Interface Sci 579:96–108

Huang Y, Chen Y, Xie J, Liu H, Yin X, Wu C (2016) Bio-oil production from hydrothermal liquefaction of high-protein high-ash microalgae including wild *Cyanobacteria* sp. and cultivated *Bacillariophyta* sp. Fuel 183:9–19

Ji C, He Z, Wang Q, Xu G, Wang S, Xu Z, Ji H (2017) Effect of operating conditions on direct liquefaction of low-lipid microalgae in ethanol-water co-solvent for bio-oil production. Energy Convers Manag 141:155–162

Jia Z, Hu J, Lu P, Wang Y (2024) Carbon quantum dots from carbohydrate-rich residue of birch obtained following lignin-first strategy. Biores Technol 408:131206

Karimi J, Asgharpour A, Mohsenzadeh S, Abbasi S (2024) The impact of polystyrene nanoplastics (PSNPs) on physiological and biochemical parameters of the microalgae *Spirulina platensis*. J Hazard Mater 474:134644

Kumar V, Jaiswal KK, Vlaskin MS, Nanda M, Tripathi MK, Gururani P, Kumar S, Joshi HC (2021) Hydrothermal liquefaction of municipal wastewater sludge and nutrient recovery from the aqueous phase. Biofuels 13(5):657–662

Lang Q, Guo Y, Zheng Q, Liu Z, Gai C (2018) Co-hydrothermal carbonization of lignocellulosic biomass and swine manure: Hydrochar properties and heavy metal transformation behavior. Bioresour Technol 266:242–248

Lee J, Lee K, Sohn D, Kim YM, Park KY (2018) Hydrothermal carbonization of lipid extracted algae for hydrochar production and feasibility of using hydrochar as a solid fuel. Energy 153:913–920

Li CS, Cai RR (2022) Preparation of solid organic fertilizer by co-hydrothermal carbonization of peanut residue and corn cob: a study on nutrient conversion. Sci Total Environ 838:155867

Li H, Shi Y, Bai L, Chi M, Xu X, Liu Y (2021a) Low temperature one-pot hydrothermal carbonization of corn straw into hydrochar for adsorbing cadmium (II) in wastewater. Energies 14(24):8503

Li HZ, Zhang YN, Guo JZ, Lv JQ, Huan WW, Li B (2021b) Preparation of hydrochar with high adsorption performance for methylene blue by co-hydrothermal carbonization of polyvinyl chloride and bamboo. Bioresour Technol 337:125442

Li P, Huang Y, Xia A, Zhu X, Zhu X, Liao Q (2023) Bio-decarbonization by microalgae: a comprehensive analysis of CO_2 transport in photo-bioreactor. DeCarbon 2:100016

Liang C, Hu X, Wang Y, Zhang Y, Fu G, Li C (2021) Study on luminescence mechanism of nitrogen-doped carbon quantum dots with different fluorescence properties and application in Fe^{3+} detection. J Nanopart Res 23(4):101

Liao LH, Qi JC, Gao J, Qu XW, Hu ZY, Fu BY, Wu FS (2024) Nitrogen-doped carbon quantum dots with photoactivation properties for ultraviolet ray detection. ACS Appl Mater Interfaces 16(32):42632–42640

Liu W, Ning C, Sang R, Hou Q, Ni Y (2021) Lignin-derived graphene quantum dots from phosphous acid-assisted hydrothermal pretreatment and their application in photocatalysis. Ind Crops Prod 171:113963

Liu X, Fan Y, Zhai Y, Liu X, Wang Z, Zhu Y, Shi H, Li C, Zhu Y (2022) Co-hydrothermal carbonization of rape straw and microalgae: pH-enhanced carbonization process to obtain clean hydrochar. Energy 257:124733

Lu J, Watson J, Liu Z, Wu Y (2022) Elemental migration and transformation during hydrothermal liquefaction of biomass. J Hazard Mater 423(Pt A):126961

Miyata Y, Fukushima T, Kihira M, Takisawa K (2022) Effect of hydrothermal reaction conditions on hydrochar from microalgae. Biomass Convers Biorefin 14:349–357

Nishshankage K, Fernandez AB, Pallewatta S, Buddhinie PKC, Vithanage M (2024) Current trends in antimicrobial activities of carbon nanostructures: potentiality and status of nanobiochar in comparison to carbon dots. Biochar 6(1):2

Rani UA, Ng LY, Ng CY, Mahmoudi E, Ng Y-S, Mohammad AW (2021) Sustainable production of nitrogen-doped carbon quantum dots for photocatalytic degradation of methylene blue and malachite green. J Water Process Eng 40:101816

Ruan Y, Wu L, Jiang X (2016) Self-assembly of nitrogen-doped carbon nanoparticles: a new ratiometric UV-vis optical sensor for the highly sensitive and selective detection of Hg^{2+} in aqueous solution. Analyst 141(11):3313–3318

Saeed AA, Harun NY, Sufian S, Siyal AA, Zulfiqar M, Bilad MR, Vagananthan A, Al-Fakih A, Ghaleb AA, Almahbashi N (2020) *Eucheuma cottonii* seaweed-based biochar for adsorption of methylene blue dye. Sustainability 12(24):10318

Sankaran R, Parra Cruz RA, Pakalapati H, Show PL, Ling TC, Chen WH, Tao Y (2020) Recent advances in the pretreatment of microalgal and lignocellulosic biomass: a comprehensive review. Bioresour Technol 298:122476

Shen Q, Zhu X, Peng Y, Xu M, Huang Y, Xia A, Zhu X, Liao Q (2024) Structure evolution characteristic of hydrochar and nitrogen transformation mechanism during co-hydrothermal carbonization process of microalgae and biomass. Energy 295:131028

Shi J, Zhou Y, Ning J, Hu G, Zhang Q, Hou Y, Zhou Y (2022a) Prepared carbon dots from wheat straw for detection of Cu^{2+} in cells and zebrafish and room temperature phosphorescent anti-counterfeiting. Spectrochim Acta A Mol Biomol Spectrosc 281:121597

Shi Y, Zhang S, Xu J, Cao Z, Wu Y (2022b) Effect of hydrothermal and hydrothermal oxidation pretreatment on the physicochemical properties of biofuel pellet. J Anal Appl Pyrolysis 165:105566

Singh R, Prakash A, Balagurumurthy B, Singh R, Saran S, Bhaskar T (2014) Hydrothermal liquefaction of agricultural and forest biomass residue: comparative study. J Mater Cycles Waste Manag 17(3):442–452

Singh AK, Singh VK, Singh M, Singh P, Khadim SR, Singh U, Koch B, Hasan SH, Asthana RK (2019) One pot hydrothermal synthesis of fluorescent NP-carbon dots derived from *Dunaliella salina* biomass and its application in on-off sensing of Hg (II), Cr (VI) and live cell imaging. J Photochem Photobiol A 376:63–72

Sui H, Liu X, Zhong F, Cheng K, Luo Y, Ju X (2014) Polyurethane thermal effects studied using two-dimensional correlation infrared spectroscopy. Polym Degrad Stab 110:13–22

Sun C, Xia A, Liao Q, Fu Q, Huang Y, Zhu X, Wei P, Lin R, Murphy JD (2018) Improving production of volatile fatty acids and hydrogen from microalgae and rice residue: effects of physicochemical characteristics and mix ratios. Appl Energy 230:1082–1092

Sun M, Xu X, Wang C, Bai Y, Fu C, Zhang L, Fu R, Wang Y (2020) Environmental burdens of the comprehensive utilization of straw: Wheat straw utilization from a life-cycle perspective. J Clean Prod 259:120702

Tsarpali M, Arora N, Kuhn JN, Philippidis GP (2021) Beneficial use of the aqueous phase generated during hydrothermal carbonization of algae as nutrient source for algae cultivation. Algal Res 60:102485

Usman M, Chen H, Chen K, Ren S, Clark JH, Fan J, Luo G, Zhang S (2019) Characterization and utilization of aqueous products from hydrothermal conversion of biomass for bio-oil and hydro-char production: a review. Green Chem 21(7):1553–1572

Varela CF, Moreno-Aldana LC, Agámez-Pertuz YY (2024) Adsorption of pharmaceutical pollutants on $ZnCl_2$-activated biochar from corn cob: efficiency, selectivity and mechanism. J Bioresour Bioprod 9(1):58–73

Wang J, Peng X, Chen X, Ma X (2019a) Co-liquefaction of low-lipid microalgae and starch-rich biomass waste: the interaction effect on product distribution and composition. J Anal Appl Pyrolysis 139:250–257

Wang X, Chen Q, Zhang Z, He H, Ma X, Liu Z, Ge B, Huang F (2019b) Novel *Enteromorpha Prolifera* based carbon dots: probing the radical scavenging of natural phenolic compounds. Colloids Surf B Biointerfaces 174:161–167

Wang T, Si B, Gong Z, Zhai Y, Cao M, Peng C (2020) Co-hydrothermal carbonization of food waste-woody sawdust blend: interaction effects on the hydrochar properties and nutrients characteristics. Bioresour Technol 316:123900

Wang Z, Lu Y, Yuan H, Ren Z, Xu C, Chen J (2015) Microplasma-assisted rapid synthesis of luminescent nitrogen-doped carbon dots and their application in pH sensing and uranium detection. Nanoscale 7(48):20743–20748

Xu X, Tu R, Sun Y, Wu Y, Jiang E, Gong Y, Li Y (2019) The correlation of physicochemical properties and combustion performance of hydrochar with fixed carbon index. Bioresour Technol 294:122053

Xu Q, Liu T, Li L, Liu B, Wang X, Zhang S, Li L, Wang B, Zimmerman AR, Gao B (2021) Hydrothermal carbonization of distillers grains with clay minerals for enhanced adsorption of phosphate and methylene blue. Bioresour Technol 340:125725

Yang J, Guo Z, Yue X (2021) Preparation of carbon quantum dots from corn straw and their application in Cu^{2+} detection. BioResources 17(1):604–615

Yao X, Ma C, Huang H, Zhu Z, Dong H, Li C, Zhang W, Yan Y, Liu Y (2018) Solvothermal-assisted synthesis of biomass carbon quantum dots/bismuth oxyiodide microflower for enhanced photocatalytic activity. NANO 13(03):1850031

Yu Y, Lau A, Sokhansanj S (2021) Improvement of the pellet quality and fuel characteristics of agricultural residues through mild hydrothermal treatment. Ind Crops Prod 169:113654

Yu S, He J, Zhang Z, Sun Z, Xie M, Xu Y, Bie X, Li Q, Zhang Y, Sevilla M, Titirici MM, Zhou H (2024) Towards negative emissions: hydrothermal carbonization of biomass for sustainable carbon materials. Adv Mater 36(18):2307412

Yuan M, Zhong R, Gao H, Li W, Yun X, Liu J, Zhao X, Zhao G, Zhang F (2015) One-step, green, and economic synthesis of water-soluble photoluminescent carbon dots by hydrothermal treatment of wheat straw, and their bio-applications in labeling, imaging, and sensing. Appl Surf Sci 355:1136–1144

Zhang JM, Zhong ZW, Zhu DP, Lin LM, Wang QJ, Tang QY, Luo ZM, Ye LY (2014) Application of bamboo shoot shell in color removal from methylene blue solution. Appl Mech Mater 675–677:489–492

Zhang J, Liu X, Zhou J, Huang X, Xie D, Ni J, Ni C (2019) Carbon dots derived from algae as H_2O_2 sensors: the importance of nutrients in biomass. Nanoscale Adv 1(6):2151–2156

Zhang CY, Ma XQ, Zheng CP, Huang T, Lu XL, Tian YL (2020a) Co-hydrothermal carbonization of water hyacinth and sewage sludge: effects of aqueous phase recirculation on the characteristics of hydrochar. Energy Fuels 34(11):14147–14158

Zhang J, Hori N, Takemura A (2020b) Thermal and time regularities during oilseed rape straw liquefaction process to produce bio-polyol. J Clean Prod 277:124015

Zhang S, Pi M, Su Y, Xu D, Xiong Y, Zhang H (2020c) Physiochemical properties and pyrolysis behavior evaluations of hydrochar from co-hydrothermal treatment of rice straw and sewage sludge. Biomass Bioenergy 140:105664

Zhang J, Xia A, Chen H, Nizami A-S, Huang Y, Zhu X, Zhu X, Liao Q (2022a) Biobased carbon dots production via hydrothermal conversion of microalgae *Chlorella pyrenoidosa*. Sci Total Environ 839:156144

Zhang J, Xia A, Yao D, Guo X, Lam SS, Huang Y, Zhu X, Zhu X, Liao Q (2022b) Removal of oxytetracycline and ofloxacin in wastewater by microalgae-bacteria symbiosis for bioenergy production. Bioresour Technol 363:127891

Zhang J, Xia A, Zhu X, Huang Y, Zhu X, Liao Q (2022c) Co-production of carbon quantum dots and biofuels via hydrothermal conversion of biomass. Fuel Process Technol 232:107276

Zhang C, Gong X, Zeng J, Peng Z, Li X, Lin L, Peng Y, Wang S (2023a) Effects of solvent phase recycling on microalgae liquefaction in ethanol: bio-oil production and nitrogen transformation. Sci Total Environ 902:166069

Zhang Q, Mu K, Han J, Qin LB, Zhao B, Yi LL (2023b) Low nitrogen and high value hydrochar preparation through co-hydrothermal carbonization of sludge and saw dust with acid/alcohol assistance. Energy 278:128012

Zhang X, Chen F, Liu S, Lou J, Liu W, Rousseau DPL, Van Hulle S (2024) Synthesis, characterization, and methylene blue adsorption isotherms of hydrochars derived from forestry waste and agro-residues. Biomass Convers Biorefin 14:1809–1824

Zhu Z, Si B, Lu J, Watson J, Zhang Y, Liu Z (2017) Elemental migration and characterization of products during hydrothermal liquefaction of cornstalk. Bioresour Technol 243:9–16

Zhu ZW, Ma SS, He SJ, Song MJ, Xia BY, You B (2025) Heterogeneous electrocatalysts from nanostructures to single atoms for biomass-derived feedstocks upgrading. Coord Chem Rev 527:216399

Zulfajri M, Kao Y-T, Huang GG (2021) Retrieve of residual waste of carbon dots derived from straw mushroom as a hydrochar for the removal of organic dyes from aqueous solutions. Sustain Chem Pharm 22:100469